Diffraction and electron energy loss to plasmons in silicon slabs

Zachary H. Levine

National Institute of Standards and Technology, Gaithersburg, Maryland 20899-8410, USA
(Received 6 June 2007; revised manuscript received 17 October 2007; published 10 March 2008)

Dynamical diffraction patterns were calculated for 25 nm slabs of silicon with [001], [111], and [110] faces for a 120 keV electron beam. The calculation used the mixed dynamical form factor in the dielectric formulation. Dielectric matrices with wave vector and frequency dependence were calculated within the local density approximation using the random phase approximation. The energy losses, $10-25$ eV, span the plasmon peak. Near the zone axes, the results show the preservation of elastic contrast and both excess and deficit Kikuchi lines.

I. INTRODUCTION

A fast electron passing through a solid is most likely to lose energy to plasmons. The energy loss is proportional to $-\text{Im}[1/\varepsilon(\vec{q},\omega)]$, which is often determined from optical measurements; this function has a prominent plasmon peak for nearly all materials. Here, $\varepsilon(\vec{q},\omega)$ is the complex dielectric function as a function of wave vector $\vec{q}$ and frequency ω. The phenomenon of diffraction by fast electrons in solids is, at least, as well known: the Davisson-Germer and Thomson-Reid experiments demonstrated that electrons are waves because they diffract from surfaces. The experiments were given a basis within quantum mechanics by Bethe,[1] which played a significant historical role in the acceptance of the notion that electrons were waves.

Both energy loss and diffraction may occur simultaneously. The preservation of diffraction contrast in the presence of electron energy loss was shown theoretically by Howie.[2] The theory was cast in terms of the mixed dynamical form factor (MDFF) by Rose[3] and later reviewed by Kohl and Rose,[4] with further development and calculations by Dudarev *et al.*,[5] by Schattschneider *et al.*,[6] and by Allen *et al.*[7,8] Recently, the MDFF was used to observe magnetic moments with non-spin-polarized electrons by considering spin-orbit coupling.[9]

Although the dielectric formulation of the MDFF is not new, there does not appear to have been a calculation of dynamical diffraction in the plasmon regime. Such a calculation is of interest from a fundamental point of view because it is necessary to consider both the wave function of the fast electron and the band structure of the solid through its dielectric function. Previous studies have tended to consider the solid through atom-based calculations, particularly for core levels. The local-field corrections to the dielectric matrix in electron energy loss in the plasmon regime have been calculated and observed for TiO_2, but without considering diffraction.[10]

For an application, consider nanotomography. To obtain chemical sensitivity, it is natural to consider electron energy loss spectra. Moreover, it is natural to consider energy loss in the plasmon regime for thin samples because the interaction length is less than for other energy losses. In small samples, diffraction is a key issue. One response is to recognize the wave mechanical nature of the signals and to perform phase retrieval. Using the oversampling method, three-dimensional phases with atomic resolution have been recovered in electron microscopy.[11] Another avenue is to use analysis methods based on incoherent illumination. If the samples are amorphous, as may frequently be achieved in biology, the sample itself ensures that the signals are incoherent. In materials science, the samples often contain crystallites. Sampling away from conditions of strong diffraction may be sufficient in this case. A recent example using electron energy loss in the plasmon regime is the tomographic reconstruction of a Si/SiO_2 system.[12] A final strategy is to use illumination conditions which are sufficiently incoherent. Recently, Levine and Dunstan proposed tapered solid-cone illumination which leads to a mutual coherence function considerably more localized than hollow-cone illumination.[13] Tomography based on projections may then be used so long as the number of voxels through the sample is smaller than the reciprocal of the full cone angle. In this work, I will generate some diffraction patterns with energy loss in the plasmon regime. It is part of an ongoing program to understand how such patterns may be used—possibly with incoherent averaging, possibly with phase retrieval—to obtain tomographic reconstructions of nanoscale objects.

II. THEORY AND COMPUTATION

I have implemented the dielectric formulation of the theory as given by Dudarev *et al.*[5,14] Their formulation, following Kohl and Rose,[4] assumes that the induced electron density in the solid is related to the induced scalar potential by the Coulomb equation, which implies that the random phase approximation (RPA) dielectric function should be used. In solid-state physics, such an assumption is known as the RPA including local-field corrections. The theory was introduced by Adler and Wiser.[15,16] A considerable body of work exists on more sophisticated dielectric functions, including exchange-correlation corrections,[17] self-energy corrections in the form of the scissors operator,[18] the Bethe-Salpeter equation,[19] and long-range corrections to adiabatic time-dependent local-density-functional theory.[20] Recently, several of these theories have been applied to newly acquired data of the dynamic form factor for silicon in the plasmon regime from inelastic x-ray scattering.[21] To couple a more sophisticated dielectric function into the formalism would

require some reformulation. The use of such a dielectric function may result in changes on the order of a factor of 2, but the qualitative features will almost surely be captured within the existing theory.

The principal elements of the theory are as follows: the fast electron is treated within single-particle nonrelativistic quantum mechanics. The sample is treated as a quantum mechanical system within band theory. Their interaction is the Coulomb interaction, neglecting exchange effects (valid if the fast electron energy is above about 1 keV) and any magnetic or relativistic effects (valid below about 200 keV). There is single scattering event, so the theory is limited to slabs thin compared to the mean free path for a volume plasmon interaction which is greater than 100 nm for 120 keV electrons in silicon. Thermal diffuse scattering is neglected.

The differential inelastic cross section is given by Eq. (DPW 21) of Ref. 5. With a slight change of notation, it is

$$\frac{d^3\sigma}{d\Omega d\omega} = \frac{k}{4\pi^2 k_0} \int d\vec{r} d\vec{r}' \rho^{(0)}_{\vec{k}\vec{k}_0}(\vec{r}) \rho^{(0)*}_{\vec{k}\vec{k}_0}(\vec{r}') \overline{s}(\vec{r}', \vec{r}, \omega). \quad (1)$$

The outgoing wave vector is $\vec{k}$, the incoming wave vector is $\vec{k}_0$, $d\Omega$ is the differential solid angle specifying the direction of the outgoing wave vector, and ω is the energy loss. I adopt atomic units ($m = \hbar = e = 1$; in this system, the unit of length is the Bohr radius and the unit of energy is the Hartree). The exchange charge is

$$\rho^{(0)}_{\vec{k}\vec{k}_0}(\vec{r}) = \psi^{(0)*}_{\vec{k}}(\vec{r}) \psi^{(0)}_{\vec{k}_0}(\vec{r}). \quad (2)$$

The wave function $\psi^{(0)}_{\vec{k}_0}(\vec{r})$ is a Bloch wave. It is discussed later.

The function $\overline{s}(\vec{r}', \vec{r}, \omega)$ is the real-space MDFF. Equation (DPW 7) of Ref. 5 relates it to the k-space MDFF, written here as

$$S(\vec{q}, \vec{q}', \omega) = \frac{q^2 q'^2}{(4\pi)^2} \int d\vec{r} d\vec{r}' e^{-i\vec{q}\cdot\vec{r} + i\vec{q}'\cdot\vec{r}'} \overline{s}(\vec{r}, \vec{r}', \omega) \quad (3)$$

with atomic units; in atomic units, the electric constant ϵ_0, found in Eq. (DPW 7) of Ref. 5, equals $(4\pi)^{-1}$. The connection to solid-state physics is given by Eq. (DPW 30) of Ref. 5, written here as

$$S(\vec{q}, \vec{q}', \omega) = \frac{i}{8\pi^2} [q^2 \varepsilon^{-1}(\vec{q}, \vec{q}', \omega) - q'^2 \varepsilon^{-1}(\vec{q}', \vec{q}, \omega)^*]. \quad (4)$$

The zero-temperature case is appropriate because we consider the excitation of plasmons. Phonons are not considered except that the static lattice potential is reduced by the Debye-Waller factor of Si at 300 K.[22] In the case of a crystal, the dielectric matrix ε and, hence, the MDFF are nonzero only if $\vec{q} - \vec{q}' = \vec{G}$ for some reciprocal lattice vector $\vec{G}$. In this case, the inverse dielectric function reduces to the form $\varepsilon^{-1}_{\vec{G}\vec{G}'}(\vec{q}, \omega)$, with $\vec{q}$ in the first Brillouin zone. By analogy, we may write the nonzero terms of the reciprocal space mixed-dynamical form factor as $S_{\vec{G}\vec{G}'}(\vec{q}, \omega)$. Equation (1) may be recast as

$$\frac{d^3\sigma}{d\Omega d\omega} = 4\frac{k}{k_0} \sum_{\vec{G}\vec{G}'} \frac{\rho_G(\vec{q})}{(\vec{q}+\vec{G})^2} S_{\vec{G}\vec{G}'}(\vec{q}, \omega) \frac{\rho^*_{\vec{G}'}(\vec{q})}{(\vec{q}+\vec{G}')^2} \quad (5)$$

using Parseval's theorem and periodicity. Equation (5) is evaluated in the code for a grid of $\vec{q}$ which spans the first Brillouin zone.

In the first stage of the calculation, a self-consistent local-density approximation (LDA) potential using pseudopotentials in a plane wave basis was found using a code described in Ref. 23, taking the silicon lattice constant a to be 543 pm, the energy cutoff to be 16 Ry, and the k-point mesh to be $4 \times 4 \times 4$. Next, the first 200 bands were determined at each of the 512 k points in the Brillouin zone. To ensure that no degenerate manifold was partially included, band 200 and any bands degenerate with it were excluded. Hence, 197–199 bands were retained. For each of the 8×8 possible transverse momentum transfers within the projected Brillouin zone, 32 longitudinal momentum transfers were calculated in the range $\pm\frac{2\pi}{a}C\hat{n}$, where $C = 2$, $\sqrt{3}$, or $\sqrt{2}$ for the [001], [111], and [110] cases, respectively. Sets of 512 k points for the four valence bands were computed with the meshes offset in $\vec{q}$ for a total of 2^{22} or about 4×10^6 wave functions. The valence bands were offset by $-\vec{q}$ rather than offsetting the conduction bands by $\vec{q}$ because there are many fewer valence bands.

Given the offset wave functions, the dielectric matrix was formed for $8 \times 8 \times 32 = 2048$ value of $\vec{q}$. The dielectric matrix rank was chosen to be 462–464 depending on the value of $\vec{q}$, which is about the same size as those considered to be fully converged by Hybertsen and Louie.[17] The matrix was evaluated using a sum-over-states method. Following the implementation in ABINIT,[24] Fourier transforms were used to evaluate the matrix elements $\langle n\vec{k}-\vec{q}|e^{i\vec{G}\cdot\vec{r}}|m\vec{k}\rangle$ for all $\vec{G}$ at once. Specifically, the code first makes the product $\langle n\vec{k} -\vec{q}|\vec{r}\rangle\langle\vec{r}|m\vec{k}\rangle$, where $\langle\vec{r}|m\vec{k}\rangle$ is the periodic part of an unoccupied wave function in real space at a point $\vec{k}$ in the Brillouin zone and $\langle\vec{r}|n\vec{k}-\vec{q}\rangle$ is the corresponding function of an occupied state at a point $\vec{k}-\vec{q}$. Then, the product is Fourier transformed to reciprocal space to make the matrix elements. The same technique is also used to make $\rho^{(0)}_{\vec{k}\vec{k}_0}(\vec{r})$ from the Bloch functions. The imaginary part was chosen to be 0.1 eV, which is appropriate given the density of k points in the Brillouin zone. Results for individual matrix elements of $\epsilon_{\vec{G}\vec{G}'}(\vec{q})$ agreed with Hybertsen and Louie, Engel and Farid,[25] and Shirley[26] to about 2% for $\vec{q}$ at the Γ point and the X point of the Brillouin zone.

Given the dielectric matrices, the MDFF was determined. In detail, the relevant momentum transfer includes the longitudinal change at the interface as determined by the dynamical diffraction equations as well as by the specified transverse momentum change. Because it was necessary to know the MDFF at a large number of closely related values, one-dimensional interpolation over the longitudinal momentum was performed for each element of ε.

Next, the Bloch waves (i.e., the wave functions for the fast electron) were determined. These functions are widely

used for elastic scattering.[14] It is sufficient to solve a one-electron Schrödinger equation because the fast electron does not have a significant exchange interaction with the medium. The wave functions satisfy the dynamic diffraction equations given initially by Bethe,[1] reviewed by Humphreys,[27] and also presented by Spence and Zuo[28] as well as by Spence[29] and Peng *et al.*[14] The principal steps in the derivation are the following: begin with a one-electron Schrodinger equation for the fast electron in a plane wave basis. The potential seen by the fast electron is taken to be the Coulomb potential arising from the charge of the nuclei and the electrons of the solid. The equation supports both forward scattering and backscattering solutions. However, backscattering is neglected, which is appropriate for transmission studies, and so the rank of the equations is halved. In band theory, the standard procedure is to obtain an eigenvalue equation in the energy for fixed crystal momentum $\vec{k}$. Here, the boundary conditions are for fixed energy and fixed component of the incident (or exiting) crystal momentum parallel to the surface. By invoking the small angle approximation,[29] a renormalization term may be neglected, leading to an eigenvalue equation for the momentum transfer normal to the surface. The equation used in the program is

$$\sum_{\vec{G}'} \left(\frac{1}{2} k_0^2 \delta_{\vec{G}\vec{G}'} + V(\vec{G} - \vec{G}') \right) C_{G'}^{(j)} = k_0 \gamma^{(j)} C_G^{(j)}, \quad (6)$$

which differs negligibly from Eq. (5.38b) of Ref. 29. In Eq. (6), k_0 is the magnitude of the wave vector of the incident electron outside the sample.

Writing the surface normal as $\hat{n}$, the wave vector of a Bloch wave in the crystal is $\vec{k} + \gamma_j \hat{n}$. The Bloch waves are of the form

$$\psi_{\vec{k}}(\vec{r}; \vec{G}_0) = e^{i\vec{k}\cdot\vec{r}} \sum_{j\vec{G}} C_{\vec{G}_0 j} e^{-i\gamma_j t} C_{j\vec{G}}^{-1} e^{i\vec{G}\cdot\vec{r}}, \quad (7)$$

where $t=0$ at the entrance face, t is the thickness at the exit face, and C is an orthogonal matrix, which are the eigenvectors of the dynamical diffraction equation. For the incident wave, $\vec{k}=\vec{k}_0$ and $G_0=0$ is selected. For the outgoing waves undergoing elastic scattering, the various $\vec{G}_0$ represent the diffraction spots. For inelastic scattering, this is still true with the proviso that the outgoing wave vector differs from the incident wave vector by $\vec{q}$ and, possibly, a reciprocal lattice vector as well, i.e., $\vec{k}_0 + \vec{q} = \vec{k} + \vec{G}_0$.

The potential seen by the fast electron was taken to be a sum of atomic Hartree-Fock potentials calculated by Shirley and arranged on the crystal lattice. These were fitted to the functional form

$$V(q) = -\frac{4\pi Z}{1+q^2} + \sum_{n=1}^{11} a_n \exp[-0.025(1.8)^n q^2], \quad (8)$$

where $Z=14$ is the atomic number, a_n are in Hartree, and q is in inverse Bohr radii. The coefficients a_n are given in Table I. This form of the fit was influenced by the work of Doyle and Turner[30] and Peng *et al.*[22] as well as the notion of even-tempered Gaussians used in quantum chemistry.[31] In the

TABLE I. Coefficients a_n (in Hartrees) of the fit to the atomic Hartree-Fock potential used in Eq. (8).

1	0.06100684636710776
2	0.3398684920695597
3	11.120934703306748
4	18.200208894138253
5	24.350051615531278
6	10.766050998069177
7	16.8737604880308
8	2.7542799447703095
9	10.23543772722582
10	−2.8423939740790876
11	2.3456589378063715

limit of large q, the fit reduces to the unscreened nuclear potential. The mean inner atomic potential was 16.7 eV, compared to 12.2–13.8 eV reported earlier based on density-functional calculations.[32] The exchange charge was determined from the fast electron wave functions using Eq. (2).

The Bloch states were represented by a basis of 113 plane waves (or "beams") about its central value. This value is sufficient to represent diffraction out to about three primitive lattice vectors. Spot checks with 59 plane waves revealed little difference in the common portion. The same energy is used for the various outgoing states regardless of their energy. For the energies used in this study, this represents the neglect of the difference between an electron with a kinetic energy of 120.000 keV and that of an electron with 119.975 keV.

Finally, the inelastic cross section was obtained by integrating the exchange charge and the MDFF according to Eq. (5). The calculation was rerun for a set of 64 wave vectors throughout the projected first Brillouin zone. The diffracted wave vectors were accumulated at the same time. The code computes cross sections for several incident angles using the same mixed-dynamical form factor up to the final interpolation.

III. RESULTS

The calculations presented in this paper are for the inelastic differential cross section of crystalline silicon slabs 25 nm thick with parallel [001], [111], or [110] faces. The fast electron energy is chosen to be 120 keV, a common energy for electron microscopy, but one which is still well in the non-relativistic regime.

The differential cross section $d^3\sigma/d\omega d\Omega$ $(\hat{k}_{in}; E, \hat{n}, t)$ is a five-dimensional function which exists for each value of the primary beam energy E, crystal face normal $\hat{n}$, and thickness t. I can only present a tiny fraction of the potential cases here, although hopefully enough to understand the essential features of the results. Additional examples are available.[33] The analogous function in elastic scattering $d^2\sigma/d\Omega$ $(\hat{k}_{in}; \hat{n}, t)$ is known as a Kikuchi map.

In Fig. 1, I present optical data[34] for $-\text{Im}[1/\epsilon(\vec{q} \approx 0, \omega)]$ vs the present calculation for the seven frequencies which
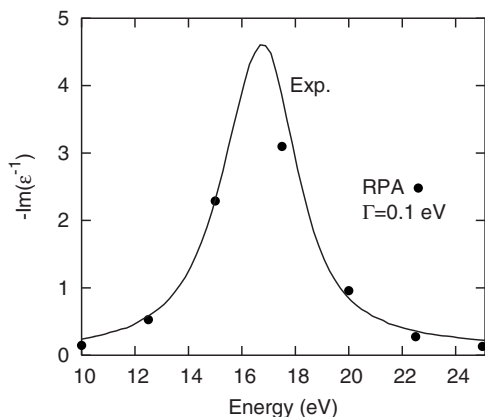
FIG. 1. The electron energy loss function $-\mathrm{Im}[1/\epsilon(\vec{q},\omega)]$ for $\vec{q} \approx 0$ from an optical experiment (Ref. 34) and the present calculation at the seven frequencies used in the paper.

were used in this study, namely, $10-25$ eV in steps of 2.5 eV. The RPA on LDA calculation gives a good account of the plasmon peak. The full width of the data at half-maximum is 3.4 eV, so 2.5 eV is a reasonable sampling interval.

In Fig. 2, $-\mathrm{Im}[1/\epsilon(\vec{q},\omega)]$ is presented for the particular value of $q = 0.8 a_0^{-1}$ along [111]. Weissker *et al.* performed an x-ray scattering experiment as well as a RPA calculation.[21] For the present calculation, two values for the full width at half-maximum parameter Γ are used, namely, 0.1 and 1.1 eV. The former value was used throughout the rest of the study. The latter value was used by Ref. 21. There are other differences between the present calculation and that of Ref. 21. For example, 512 vs 2048 k points, 113 vs 51–89 $\vec{G}$ for the dielectric matrix, 464–483 vs 89–259 $\vec{G}$ vectors for the wave function, and 197–199 vs 70–200 bands for the present calculation vs that of Ref. 21, respectively. The results suggest that the present calculation could be subject to correc-
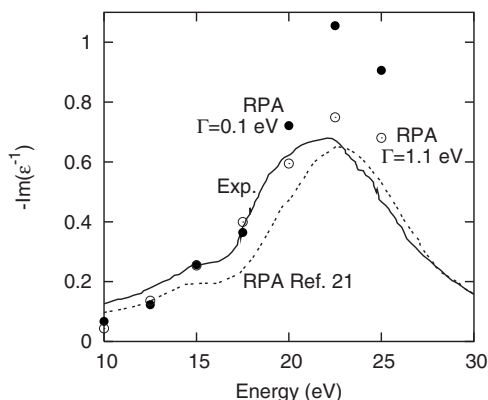
FIG. 2. The electron energy loss function $-\mathrm{Im}[1/\epsilon(\vec{q},\omega)]$ for $\vec{q} = 0.8 a_0^{-1}$ along the [111] direction, from an x-ray scattering experiment (Ref. 21), a RPA calculation (Ref. 21), and the present calculation at the seven frequencies used in the paper, with two values for the full width at half-maximum Γ. The value of 0.1 eV was used throughout this work. The value of 1.1 eV matches the calculation of Ref. 21.

tions of up to a factor of 2 if a fully converged numerical result were obtained or if a more advanced dielectric function were used. However, qualitative features are given correctly, including, in particular, the $\vec{q}$-dependent position of the plasmon peak.

In Fig. 3, I present the differential cross section for the [001] surface, with the beam at and near the surface normal. The preservation of diffraction contrast[2] relative to elastic scattering is seen. The diffraction spots are always commensurate with the lattice. The angular scale is given by the ratio of the projected reciprocal lattice vector to the incident wave vector. For the [001] faces, the former is 23.15 nm^{-1} vs 1774 nm^{-1} for a fast electron energy of 120 keV, so the characteristic angle is 13 mrad. The incident wave vector must change by this amount for there to be a large change in the diffraction pattern. Calculations performed with steps of 0.2 mrad showed minimal variation.[33] For the [111] and [110] faces, the characteristic angle is smaller by a factor of $\sqrt{3}/2$ and $1/\sqrt{2}$, respectively.

The diffraction spots are strongest at the peak of the plasmon near 17.5 eV, and diminish for both higher and lower energies. The second prominent feature is the presence of lines which shift relative to the lattice as the incident angle is varied. These lines are known as Kikuchi lines and are usually studied in the context of thermal diffuse scattering. The intensity of the Kikuchi lines peaks near 22.5 eV, suggesting that the dispersion of the plasmon[35] plays a role. The additive Kikuchi lines are more common, but certain diffraction patterns presented here contain Kikuchi deficit lines. Examples are the highest two energy losses (top two rows) for an incident wave vector in the [0.0066, 0, 1] direction (column 3 of Fig. 3).

Wang has also calculated the diffraction pattern for a [100] silicon slab 54.3 nm thick, with an electron at normal incidence and an electron energy loss, using a semiempirical model for the dielectric function and the multislice method.[36] The Kikuchi lines appearing between the elastic diffraction spots are also a feature of his calculation, as shown in Fig. 10(a) of Ref. 36, which is similar to the case of a 15 eV energy loss in the first column of Fig. 3.

The features described above are characteristic of both the [001]-cut slab and [111]-cut slab (shown in Fig. 4); namely, the preservation of diffraction contrast, the additive and subtractive Kikuchi lines, the peak of the elastic-preserving scattering at a lower energy than the peak intensity of the Kikuchi lines. The images at normal incidence or 3 mrad for a 15 or 17.5 eV loss are similar to the experimental image presented in Fig. 8(c) of Ref. 37 for a 16 eV loss through a 50 nm slab of [111]-cut silicon.

The effect of the off-diagonal terms of the MDFF on the cross section is 1% or less. The Frobenius norm of the diagonal elements of the matrices $S_{\vec{G}\vec{G}'}(\vec{q})$ for a given $\vec{q}$ is from 70% to 84% of the Frobenius norm of the full matrix. Hence, it is somewhat surprising that the effect on the cross section is not larger. However, Howie[2] determined that elastic contrast should be preserved in plasmon energy loss, which is consistent with the present calculation. Presumably for more complicated unit cells, the local-field effects will be larger and the off-diagonal terms of the MDFF will become more prominent. The off-diagonal terms in the dielectric matrix
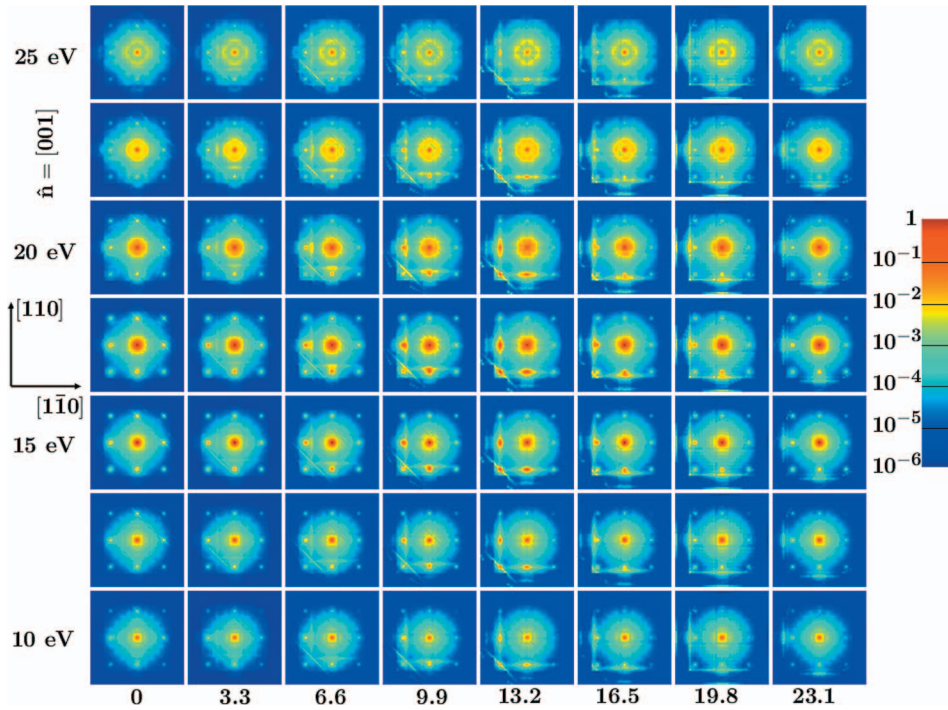
FIG. 3. (Color) Differential cross sections for the [001]-cut slab with a logarithmic scale bar given at the right. Each set of images is normalized to the maximum value in the figure as a whole. The minimum value is set to 10^{-6} of the maximum value. In each column, the angle of incidence is fixed, from normal incidence to 23.1 mrad in the [100] direction in steps of 3.3 mrad. In each row, the electron energy loss is fixed from 10 eV at the bottom to 25 eV at the top, in steps of 2.5 eV. The bright spots are coincident with the projected reciprocal lattice, which sets the scale of the momentum transfer (see text). The horizontal and vertical axes in the figure represent a momentum transfer to the outgoing beam in the [1$\bar{1}$0] and [110] directions, respectively.

$\epsilon_{\vec{G}\vec{G}'}(\vec{q})$ (i.e., local-field effects) are included even in the diagonal elements of the MDFF via $\epsilon_{\vec{G}\vec{G}'}^{-1}(\vec{q})$, similar to the calculations of Vast *et al.*[10] and Weissker *et al.*[21]

Note that Figs. 3 and 4 are centered on the incident beam. If two panels were excited simultaneously with incoherent incident beams, the resulting images would appear on a detector offset relative to each other. This leads to the possibility of incoherent averaging of the diffraction contrast in certain circumstances.[13] The elimination of diffraction contrast would require averaging over incident beam angles on the order of a reciprocal lattice vector divided by the incident wave vector.

The case of the [110] surface normal is shown in Fig. 4 in the final column. The increase of the intensity of the diffraction spots at the plasmon peak is the most prominent feature. Away from normal incidence, the interpretation is complicated by the strong elastic diffraction. The features are not so clearly identifiable in this case, although the preservation of elastic contrast and the Kikuchi lines certainly play a role in understanding the images.

IV. CONCLUSIONS

Differential cross sections with electron energy loss for the scattering of a 120 keV electron through 25 nm thick
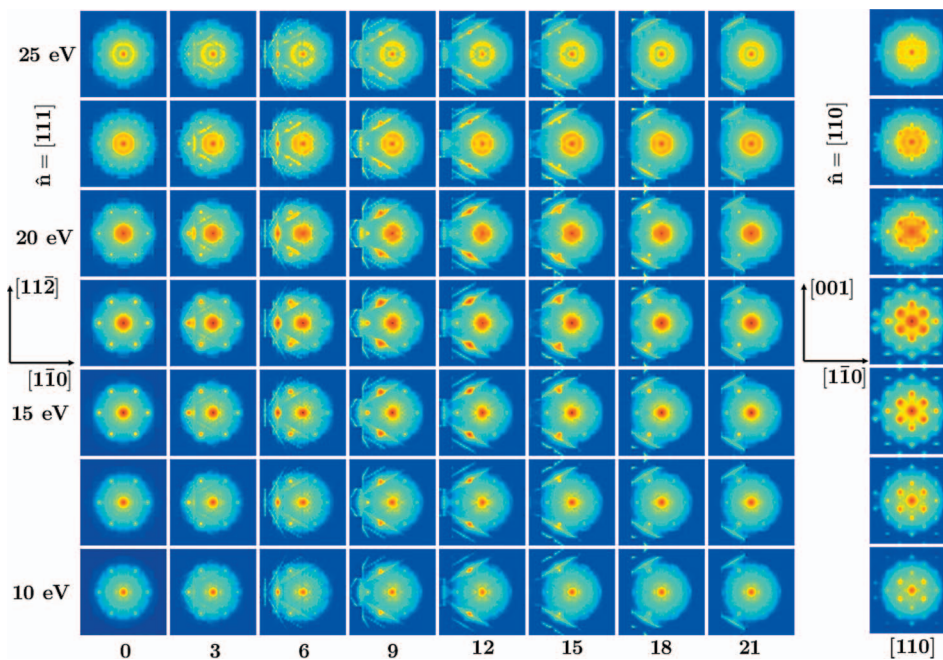
FIG. 4. (Color) Differential cross sections for the [111]-cut and [110]-cut slabs with conventions as in Fig. 3. The normalization is performed separately for each slab. The angle of incidence goes from the [111] axis toward the [1$\bar{1}$0] direction in steps of $(2\sqrt{2/3})3$ mrad ≈ 2.83 mrad except for the [110] results shown in the final column, which has normal incidence. The label omits the prefactor. The horizontal and vertical axes in the figure represent a momentum transfer to the outgoing beam in the [1$\bar{1}$0] and [11$\bar{2}$] directions, respectively, for the [111] case, and in the [1$\bar{1}$0] and [001] directions for the [110] case.

slabs of silicon have been calculated. The theory used the dynamical diffraction equations to generate elastic scattering states known as Bloch waves. Pseudopotentials and plane waves were used to generate the dielectric function of the solid which, in the RPA, is sufficient to determine the MDFF. The Bloch waves undergo a single scattering event, including energy loss, as mediated by the MDFF. The diffraction patterns near the normal directions are dominated by the preserved elastic contrast. The characteristic angle for large changes in the patterns as a function of the incident direction of the crystal is given by the ratio of a projected primitive reciprocal vector to the incident wave vector.

[1] H. A. Bethe, Ann. Phys. **87**, 55 (1928).

[2] A. Howie, Proc. R. Soc. London, Ser. A **271**, 268 (1963).

[3] H. Rose, Optik (Jena) **45**, 139 (1976); **45**, 187 (1976).

[4] H. Kohl and H. Rose, Adv. Electron. Electron Phys. **65**, 173 (1986).

[5] S. L. Dudarev, L.-M. Peng, and M. J. Whelan, Phys. Rev. B **48**, 13408 (1993). Equations (DPW 7), (DPW 21), and (DPW 30) refer to equations in this reference with the corresponding number.

[6] P. Schattschneider, M. Nelhiebel, H. Souchay, and B. Jouffrey, Micron **31**, 333 (2000).

[7] L. J. Allen, S. D. Findlay, A. R. Lupini, M. P. Oxley, and S. J. Pennycook, Phys. Rev. Lett. **91**, 105503 (2003).

[8] M. P. Oxley, E. C. Cosgriff, and L. J. Allen, Phys. Rev. Lett. **94**, 203906 (2005).

[9] P. Schattschneider, S. Rubino, C. Hebert, J. Rusz, J. Kunes, P. Novak, E. Carlino, M. Fabrizioli, G. Panaccione, and G. Rossi, Nature (London) **441**, 486 (2006).

[10] N. Vast, L. Reining, V. Olevano, P. Schattschneider, and B. Jouffrey, Phys. Rev. Lett. **88**, 037601 (2002).

[11] J. Miao, T. Ohsuna, O. Terasaki, K. O. Hodgson, and M. A. O'Keefe, Phys. Rev. Lett. **89**, 155502 (2002).

[12] A. Yurtsever, M. Weyland, and D. A. Muller, Appl. Phys. Lett. **89**, 151920 (2006).

[13] Z. H. Levine and R. M. Dunstan, J. Opt. Soc. Am. A **24**, 2402 (2007).

[14] L.-M. Peng, S. L. Dudarev, and M. J. Whelan, *High-Energy Electron Diffraction and Microscopy* (Oxford University Press, Oxford, 2004), Chaps. 3, 4, and 7. My Eqs. (1), (3), and (4) are their Eqs. (7.35), (7.58), and (7.59), respectively.

[15] S. L. Adler, Phys. Rev. **126**, 413 (1962).

[16] N. Wiser, Phys. Rev. **129**, 62 (1963).

[17] M. S. Hybertsen and S. G. Louie, Phys. Rev. B **35**, 5585 (1987).

[18] Z. H. Levine and D. C. Allan, Phys. Rev. Lett. **63**, 1719 (1989).

[19] L. X. Benedict, E. L. Shirley, and R. B. Bohn, Phys. Rev. B **57**, R9385 (1998).

[20] S. Botti, A. Schindlmayr, R. D. Sole, and L. Reining, Rep. Prog. Phys. **70**, 357 (2007).

[21] H.-C. Weissker, J. Serrano, S. Huotari, F. Bruneval, F. Sottile, G. Monaco, M. Krisch, V. Olevano, and L. Reining, Phys. Rev. Lett. **97**, 237602 (2006).

[22] L.-M. Peng, G. Ren, S. L. Dudarev, and M. J. Whelan, Acta Crystallogr., Sect. A: Found. Crystallogr. **A52**, 456 (1998).

[23] E. L. Shirley, L. J. Terminello, J. E. Klepeis, and F. J. Himpsel, Phys. Rev. B **53**, 10296 (1996).

[24] X. Gonze *et al.*, Comput. Mater. Sci. **25**, 478 (2002).

[25] G. E. Engel and B. Farid, Phys. Rev. B **47**, 15931 (1993).

[26] E. L. Shirley (private communication).

[27] C. J. Humphreys, Rep. Prog. Phys. **42**, 1825 (1979).

[28] J. C. H. Spence and J. M. Zuo, *Electron Microdiffraction* (Plenum, New York, 1992).

[29] J. C. H. Spence, *High-Resolution Electron Microscopy*, 3rd ed. (Oxford University Press, Oxford, 2003), pp. 111–113.

[30] P. A. Doyle and P. S. Turner, Acta Crystallogr., Sect. A: Cryst. Phys., Diffr., Theor. Gen. Crystallogr. **A24**, 390 (1968).

[31] M. W. Schmidt and K. Ruedenberg, J. Chem. Phys. **71**, 3951 (1979).

[32] M. Y. Kim, J. M. Zuo, and J. C. H. Spence, Phys. Status Solidi A **166**, 445 (1998).

[33] See EPAPS Document No. E-PRBMDO-77-049808 for the results in numerical form as well as additional cases. For more information on EPAPS, see http://www.aip.org/pubservs/epaps.html.

[34] C. Tarrio and S. E. Schnatterly, J. Opt. Soc. Am. B **10**, 952 (1993).

[35] A. J. Forsyth, T. W. Josefsson, and A. E. Smith, Phys. Rev. B **54**, 14355 (1996).

[36] Z. L. Wang, Acta Crystallogr., Sect. A: Found. Crystallogr. **A48**, 674 (1992).

[37] L. Reimer, I. Fromm, and I. Naundorf, Ultramicroscopy **32**, 80 (1990).